ELSEVIER

Computer Physics Communications 111 (1998) 59–75

Computer Physics Communications

Continuum Solvation Model: computation of electrostatic forces from numerical solutions to the Poisson–Boltzmann equation

Wonpil Im [a], Dmitrii Beglov [b], Benoît Roux [a,b,1]

[a] *Départements de Physique & Chimie, Université de Montréal, C.P. 6128, Succ. Centre-Ville, Canada H3C 3J7*

[b] *CERCA, Centre de Recherche en Calcul Appliquée, Boulevard Décarie, Bureau 400, Montréal, Québec, Canada H3X 2H9*

Received 3 November 1997

Abstract

A rigorous formulation of the solvation forces (first derivatives) associated with the electrostatic free energy calculated from numerical solutions of the linearized Poisson–Boltzmann equation on a discrete grid is described. The solvation forces are obtained from the formal solution of the linearized Poisson–Boltzmann equation written in terms of the Green function. An intermediate region for the solute–solvent dielectric boundary is introduced to yield a continuous solvation free energy and accurate solvation forces. A series of numerical tests show that the calculated forces agree extremely well with finite-difference derivatives of the solvation free energy. To gain a maximum efficiency, the nonpolar contribution to the free energy is expressed in terms of the discretized grid used for the electrostatic problem. The current treatment of solvation forces can be used to introduce the influence of a continuum solvation model in molecular mechanics calculations of large biological systems. © 1998 Published by Elsevier Science B.V.

1. Introduction

Considerable efforts are currently devoted to developing accurate and effective computational approaches for incorporating solvent effects implicitly in atomistic simulations of biomolecules. Macroscopic continuum electrostatics approaches based upon the Poisson–Boltzmann (PB) equation, in which the solvent is represented as a featureless dielectric material, are of particular interest [1–3]. Numerical solutions of the PB equation based on finite-difference or finite-element methods with a discretized grid can be obtained routinely in the case of molecules of irregular shapes [1–8]. Calculations based on computer simulations with explicit solvent molecules showed that the dominant electrostatic contribution to the solvation free energy of large number of small solutes [5] and the 20 standard amino acids [9] can be accurately reproduced by numerical solutions to the PB equation. Continuum electrostatics is particularly appealing because it relies on approximations that have a clear microscopic significance. For instance, it has been shown that the Poisson equation for macroscopic media follows from statistical mechanical theories of solvation in the limit where typical correlation lengths

[1] E-mail: rouxb@plgcn.umontreal.ca

PII S0010-4655(98)00016-2

in the solvent become very small [10]. For this reason, continuum electrostatics represents an effective and physically sound approach which makes it possible to account for a number of phenomena involving solvent electrostatic effects on the function of biological macromolecules.

In most practical applications, the PB equation is solved numerically for a fixed conformation of the solute and the free energy of solvation is calculated [1–3,5,9]. However, this procedure has obvious limitations since it ignores the importance of conformational flexibility of the solute. Extension of the current methodology requires the calculations of the "solvation forces", i.e., the first derivatives of the solvation free energy with respect to the atomic coordinates of the solute. For example, the forces can be used to relax the initial geometry of the solute with energy minimization and make it possible to sample the conformational space using dynamical trajectories or force-biased Monte Carlo algorithms [11,12].

Several treatments have been proposed to compute the forces associated with a continuum electrostatics description of the solvent [13–17]. Gilson et al. [16,17] pointed out a number of limitations in the previous attempts and presented an elegant treatment based upon a variational differentiation of an electrostatic energy density functional. Exact expressions were obtained for the electrostatic solvation forces. However, those expressions are rigorously valid only in the limit of an infinite grid with infinitesimal grid mesh. In the context of numerical calculations based upon the PB equation, the expressions for the electrostatic solvation forces are not explicitly equivalent to the derivative of the calculated electrostatic free energy with respect to the atomic coordinates of the solute. This implies that the calculated free energy does not correspond to the integrated work done by the forces and that the energy may be poorly conserved during dynamical trajectories. In this paper, we present a different view of the calculation of the forces based on the finite-difference PB equation. It is shown that the current expressions for the forces are equivalent to those of Gilson et al. [16,17] in the limit of an infinite grid with infinitesimal grid mesh. However, in the present treatment the forces are explicitly equal to the first derivative of the finite-difference continuum electrostatic free energy with respect to the coordinate of the solute atoms. The current expressions for the solvation forces are simple and may easily be added to current source codes solving the PB equation on a discretized grid. We chose to base the current treatment on the finite-difference PB equation although other treatments of continuum electrostatics based on boundary element techniques have also been proposed [18,19]. One reason is that the boundary conditions required by complex environments such as membrane systems are more easily implemented using the PB equation [20].

In the next section, the expressions for the electrostatic and nonpolar solvation forces are obtained. The current expressions for the solvation forces are compared with those obtained previously. The numerical implementation of the method is then presented in detail and accuracy tests are described. Finally, a molecular dynamics simulation of the alanine dipeptide is performed to illustrate the method.

2. Theoretical developments

We consider a molecular solute in a fixed configuration immersed in a polar solvent containing mobile ions. The conformation of the solute is described by the set of Cartesian coordinates $\{r_\alpha\}$. The solvation free energy of the solute in this fixed conformation may be expressed as the reversible thermodynamic work in a step-by-step process. In a first step, the neutral solute is inserted in the solvent. In a second step, the electrostatic interactions between the solute and the solvent are switched on. Thus, the solvation free energy is expressed as the sum of nonpolar contributions (np) including the cavity formation energy in the solvent and the solvent-solute van der Waals interaction energy, and electrostatic contributions (elec),

$$\Delta G_{\text{solv}} = \Delta G_{\text{np}} + \Delta G_{\text{elec}} . \tag{1}$$

Typically, the nonpolar contribution to the solvation free energy is represented as the product of the surface of the solute, S, and a phenomenological surface tension coefficient, γ [14,16,21,22],

$$\Delta G_{\rm np} = \gamma S . \tag{2}$$

Assuming a linear response during the charging process [1–3], the electrostatic contribution to the solvation free energy is calculated from the solvent reaction field. The latter is obtained by subtracting the electrostatic potential computed in vacuum ($\phi_{\rm v}$) from the total electrostatic potential computed in the solvent medium ($\phi_{\rm s}$),

$$\Delta G_{\rm elec} = \tfrac{1}{2} \sum_{\alpha} Q_\alpha \left[\phi_{\rm s}(r_\alpha) - \phi_{\rm v}(r_\alpha) \right] , \tag{3}$$

where Q_α is the charge of atom α. The electrostatic potential $\phi(r)$ is calculated by solving the linear Poisson–Boltzmann (PB) equation [1–3],

$$\nabla \cdot [\epsilon(r) \nabla \phi(r)] - \bar{\kappa}^2(r) \phi(r) = -4\pi \rho(r) , \tag{4}$$

where $\epsilon(r)$, $\bar{\kappa}(r)$, and $\rho(r)$ are the dielectric constant, the modified Debye–Hückel screening factor, and the fixed charge density of the solute, respectively. The electrostatic potential computed in vacuum is obtained by setting the dielectric constant equation to one at all points in space. The electrostatic potential computed in the solvent environment is obtained by setting the dielectric constant to one in the interior of the solute and to $\epsilon_{\rm s}$ at all points in space in the solvent region. In Eq. (4), the dielectric constant at a point, r, is defined as a function of the position of all the atoms, $\{r_\alpha\}$, in the system

$$\epsilon(r) = 1 + (\epsilon_{\rm s} - 1) H(r; \{r_\alpha\}) , \tag{5}$$

where $\epsilon_{\rm s}$ is the dielectric constant of the solvent and $H(r)$ is a volume exclusion function, equal to one in the solvent region and zero in the interior of the solute [10]. There are several conventions to construct the volume exclusion function and define the dielectric regions (see the discussion in [9]). In the current treatment, $H(r)$ is defined in terms of overlapping atomic spherical functions,

$$\begin{aligned} H(r; \{r_\alpha\}) &= \exp\left[- \sum_{\alpha} \frac{u_\alpha(|r - r_\alpha|)}{k_{\rm B} T} \right] \\ &= \prod_{\alpha} H_\alpha(|r - r_\alpha|) , \end{aligned} \tag{6}$$

where $k_{\rm B}$ is Boltzmann's constant, T is the absolute temperature, $u_\alpha(|r - r_\alpha|)$ is a spherical energy function and $H_\alpha(|r - r_\alpha|)$ is a radially symmetric atomic volume exclusion function that describes the distribution of solvent particles around atom α. This prescription for the construction of $\epsilon(r)$ differs with previous treatments in which the molecular surface of the solute was used [14,16,22]. Nevertheless, it is consistent with a statistical mechanical analysis of solvation which showed that the value of the dielectric function should be assigned on the basis of a volume exclusion function [10]. A similar definition can be used for the modified Debye–Hückel screening factor, $\bar{\kappa}(r)$,

$$\bar{\kappa}^2(r) = \bar{\kappa}_b^2 H(r; \{r_\alpha\}) , \tag{7}$$

where $\bar{\kappa}_b$ is the screening factor of an electrolyte at the bulk solvent. We have implicitly assumed that the volume excluding function of the solvent dielectric and the counterions were identical, although this approximation is not essential. In summary, the free energy $\Delta G_{\rm solv}$ depends on the coordinates of the solute through the charge distribution $\rho(r)$ and the spatial variations of the function $\epsilon(r)$ and $\bar{\kappa}(r)$. The goal is to obtain analytical expressions for the derivatives of $\Delta G_{\rm solv}$ as a function of the atomic coordinates of the solute molecule, i.e., $\partial \Delta G_{\rm solv} / \partial r_\alpha$.

2.1. Electrostatic solvation forces

In finite-difference calculations, the linear PB equation is expressed as [1,2]

$$\begin{aligned}&\epsilon_x(i,j,k)[\phi(i+1,j,k)-\phi(i,j,k)]+\epsilon_x(i-1,j,k)[\phi(i-1,j,k)-\phi(i,j,k)]\\&+\epsilon_y(i,j,k)[\phi(i,j+1,k)-\phi(i,j,k)]+\epsilon_y(i,j-1,k)[\phi(i,j-1,k)-\phi(i,j,k)]\\&+\epsilon_z(i,j,k)[\phi(i,j,k+1)-\phi(i,j,k)]+\epsilon_z(i,j,k-1)[\phi(i,j,k-1)-\phi(i,j,k)]\\&-\bar{\kappa}^2(i,j,k)\phi(i,j,k)h^2=-4\pi\frac{q(i,j,k)}{h},\end{aligned} \tag{8}$$

where h is the grid spacing, $\phi(i,j,k)$ is the electrostatic potential, $\bar{\kappa}(i,j,k)$ is the modified Debye–Hückel screening factor, and $q(i,j,k)$ is the fractional charge at the grid point (x_i,y_j,z_k). The fractional charge is related to the density at the grid points through $\rho(i,j,k) = q(i,j,k)/h^3$. The arrays $\epsilon_x(i,j,k)$, $\epsilon_y(i,j,k)$, and $\epsilon_z(i,j,k)$ represent the dielectric constants associated with the x-, y-, and z-directions grid branches, $(x_i+h/2,y_j,z_k)$, $(x_i,y_j+h/2,z_k)$, and $(x_i,y_j,z_k+h/2)$ originating at the grid point (x_i,y_j,z_k). Equivalently, Eq. (8) may be expressed as a formal linear algebra problem,

$$\mathbf{M}\cdot\boldsymbol{\phi}=-4\pi\boldsymbol{q}, \tag{9}$$

where $\mathbf{M}$ is a symmetric matrix, and $\boldsymbol{\phi}$ and $\boldsymbol{q}$ are column vectors associated with the electrostatic potentials and the fractional charges, respectively, whose number of elements is equal to the number of grid points. Even though this is not explicitly stated by the notation, it is understood implicitly that both the $\mathbf{M}$ matrix and the charge vector $\boldsymbol{q}$ are functions of the atomic positions $\{\boldsymbol{r}_\alpha\}$ of the solute. The formal solution to Eq. (9) is expressed as

$$\boldsymbol{\phi}=-4\pi\mathbf{M}^{-1}\cdot\boldsymbol{q}. \tag{10}$$

The inverse matrix $\mathbf{M}^{-1}$ corresponds to the Green's function to the finite-difference equation (8). From Eqs. (3) and (10), the electrostatic contribution to the solvation free energy is given by

$$\begin{aligned}\Delta G_{\text{elec}}&=\tfrac{1}{2}(\boldsymbol{\phi}_{\text{s}}^{\text{t}}-\boldsymbol{\phi}_{\text{v}}^{\text{t}})\cdot\boldsymbol{q}\\&=\tfrac{1}{2}(-4\pi\boldsymbol{q}^{\text{t}})\cdot(\mathbf{M}_{\text{s}}^{-1}-\mathbf{M}_{\text{v}}^{-1})\cdot\boldsymbol{q},\end{aligned} \tag{11}$$

where the superscript "t" indicates the transposed associated vector. The electrostatic solvation force acting on atom α of the solute is given by

$$\begin{aligned}\mathbf{F}_\alpha^{\text{elec}}&=-\frac{\partial\Delta G_{\text{elec}}}{\partial\boldsymbol{r}_\alpha}\\&=2\pi\frac{\partial}{\partial\boldsymbol{r}_\alpha}\left[\boldsymbol{q}^{\text{t}}\cdot(\mathbf{M}_{\text{s}}^{-1}-\mathbf{M}_{\text{v}}^{-1})\cdot\boldsymbol{q}\right]\\&=2\pi\left[\frac{\partial\boldsymbol{q}^{\text{t}}}{\partial\boldsymbol{r}_\alpha}\cdot(\mathbf{M}_{\text{s}}^{-1}-\mathbf{M}_{\text{v}}^{-1})\cdot\boldsymbol{q}+\boldsymbol{q}^{\text{t}}\cdot(\mathbf{M}_{\text{s}}^{-1}-\mathbf{M}_{\text{v}}^{-1})\cdot\frac{\partial\boldsymbol{q}}{\partial\boldsymbol{r}_\alpha}+\boldsymbol{q}^{\text{t}}\cdot\frac{\partial\mathbf{M}_{\text{s}}^{-1}}{\partial\boldsymbol{r}_\alpha}\cdot\boldsymbol{q}\right],\end{aligned} \tag{12}$$

where $\partial\mathbf{M}_{\text{v}}^{-1}/\partial\boldsymbol{r}_\alpha=0$ since the dielectric constant function of the reference vacuum system is uniform through all space ($\epsilon_{\text{v}}=1$). Using the identities

$$\frac{\partial\boldsymbol{q}^{\text{t}}}{\partial\boldsymbol{r}_\alpha}\cdot(\mathbf{M}_{\text{s}}^{-1}-\mathbf{M}_{\text{v}}^{-1})\cdot\boldsymbol{q}=\boldsymbol{q}^{\text{t}}\cdot(\mathbf{M}_{\text{s}}^{-1}-\mathbf{M}_{\text{v}}^{-1})\cdot\frac{\partial\boldsymbol{q}}{\partial\boldsymbol{r}_\alpha}, \tag{13}$$

and

$$\frac{\partial \mathbf{M}_s^{-1}}{\partial \boldsymbol{r}_\alpha} = -\mathbf{M}_s^{-1} \cdot \frac{\partial \mathbf{M}_s}{\partial \boldsymbol{r}_\alpha} \cdot \mathbf{M}_s^{-1}, \tag{14}$$

it is possible to express Eq. (12) as

$$\begin{aligned}\mathbf{F}_\alpha^{\text{elec}} &= 4\pi \boldsymbol{q}^t \cdot [\mathbf{M}_s^{-1} - \mathbf{M}_v^{-1}] \cdot \frac{\partial \boldsymbol{q}}{\partial \boldsymbol{r}_\alpha} - \frac{1}{8\pi}(4\pi \boldsymbol{q}^t \cdot \mathbf{M}_s^{-1}) \cdot \frac{\partial \mathbf{M}_s}{\partial \boldsymbol{r}_\alpha} \cdot (4\pi \mathbf{M}_s^{-1} \cdot \boldsymbol{q}) \\ &= -(\boldsymbol{\phi}_s^t - \boldsymbol{\phi}_v^t) \cdot \frac{\partial \boldsymbol{q}}{\partial \boldsymbol{r}_\alpha} - \frac{1}{8\pi} \boldsymbol{\phi}_s^t \cdot \frac{\partial \mathbf{M}_s}{\partial \boldsymbol{r}_\alpha} \cdot \boldsymbol{\phi}_s \end{aligned} \tag{15}$$

(the identity equation (13) follows from the fact that the matrix $\mathbf{M}$ is perfectly symmetric). In the limit of infinitesimal grid spacing, the forces may be expressed in terms of continuous integrals,

$$\mathbf{F}_\alpha^{\text{elec}} = -\int_V d^3\boldsymbol{r} \left[(\phi_s - \phi_v) \frac{\partial \rho}{\partial \boldsymbol{r}_\alpha} + \frac{1}{8\pi} \phi_s \nabla \cdot \left(\frac{\partial \epsilon_s}{\partial \boldsymbol{r}_\alpha} \nabla \phi_s \right) - \frac{1}{8\pi} \phi_s^2 \frac{\partial \bar{\kappa}^2}{\partial \boldsymbol{r}_\alpha} \right]. \tag{16}$$

The total electrostatic solvation force is given by the sum of three terms, $\mathbf{F}_\alpha^{\text{elec}} = \mathbf{F}_\alpha^{\text{RF}} + \mathbf{F}_\alpha^{\text{DB}} + \mathbf{F}_\alpha^{\text{IB}}$. The first term in Eq. (16) corresponds to the "reaction field force"

$$\mathbf{F}_\alpha^{\text{RF}} = -\int_V d^3\boldsymbol{r} \, (\phi_s - \phi_v) \frac{\partial \rho}{\partial \boldsymbol{r}_\alpha}. \tag{17}$$

The second term in Eq. (16),

$$\mathbf{F}_\alpha^{\text{DB}} = -\frac{1}{8\pi} \int_V d^3\boldsymbol{r} \, \phi_s \nabla \cdot \left[\frac{\partial \epsilon}{\partial \boldsymbol{r}_\alpha} \nabla \phi_s \right], \tag{18}$$

arises from the spatial variations of the dielectric constant function $\epsilon(\boldsymbol{r})$. The last term in Eq. (16),

$$\mathbf{F}_\alpha^{\text{IB}} = \frac{1}{8\pi} \int_V d^3\boldsymbol{r} \, \phi_s^2 \frac{\partial \bar{\kappa}^2}{\partial \boldsymbol{r}_\alpha}, \tag{19}$$

arises from the spatial variation of the modified Debye–Hückel screening factor $\bar{\kappa}(\boldsymbol{r})$, $\mathbf{F}_\alpha^{\text{DB}}$ and $\mathbf{F}_\alpha^{\text{IB}}$, will be refereed to as the "dielectric boundary force" and the "ionic boundary force", respectively.

The expression for the electrostatic solvation forces given in Eqs. (17) and (18) are closely related to those obtained previously by Gilson et al. [16], using a variational principle based on the electrostatic free energy functional. For instance, it can easily be shown, using the fact that the total charge density is constituted of a superposition of atomic charge densities $\rho(\boldsymbol{r}) = \sum_\alpha \rho_\alpha(|\boldsymbol{r} - \boldsymbol{r}_\alpha|)$, that Eq. (17) corresponds to the force arising from the interaction of the charge of atom α with the total electric field (due to the dielectric and counterions polarization in the solvent region in response to all the solute charges). From the identity $\partial \rho(\boldsymbol{r}) / \partial \boldsymbol{r}_\alpha = -\nabla \rho_\alpha(\boldsymbol{r})$, the reaction field force is written as

$$\begin{aligned}\mathbf{F}_\alpha^{\text{RF}} &= -\int_V d^3\boldsymbol{r} \, [\nabla(\phi_s - \phi_v)] \rho_\alpha + \int_V d^3\boldsymbol{r} \, \nabla [\rho_\alpha(\phi_s - \phi_v)] \\ &= -\int_V d^3\boldsymbol{r} \, [\nabla(\phi_s - \phi_v)] \rho_\alpha + \int_S d^2\boldsymbol{r} \, \boldsymbol{n} [\rho_\alpha(\phi_s - \phi_v)] \\ &= -\int_V d^3\boldsymbol{r} \, [\nabla(\phi_s - \phi_v)] \rho_\alpha \end{aligned} \tag{20}$$

(the surface term arising from the integration by parts does not contribute because the charge density is zero at infinity). Eq. (20) is the expression of the reaction field force used previously [14–17]. Similarly, the expression of Gilson et al. [16] for the dielectric and ionic boundary forces are recovered after integration of Eqs. (18) and (19) by parts using the divergence theorem and neglecting the surface terms. This shows that both approaches are formally identical in the limit of infinitesimal grid spacing and infinitely large box size. However, in the context of numerical calculations the two approaches can yield different results. In particular, the calculation of the reaction field force based on Eq. (20) requires the electrostatic field at the grid points (i,j,k). However, because the finite-difference algorithm based on Eq. (8) is developed by assuming that the fields are known at the mid-point along the branches [1,2], the electrostatic field at the grid points (i,j,k) are not readily available from the numerical solution. One possibility is to estimate the electric field at the grid point (i,j,k) from the value of the electrostatic potential in the neighboring grid points $(i+1,j,k)$, $(i-1,j,k)$, $(i,j+1,k)$, $(i,j-1,k)$,..., etc. However, such an estimate is associated with an error of low order in the grid spacing h, which is not consistent with the accuracy of the finite-difference algorithm based on Eq. (8). Such problems are avoided with Eq. (17) because the field is not required to calculate the reaction field forces.

2.2. Nonpolar solvation forces

To gain maximum efficiency it is desirable to express the nonpolar contribution to the solvation forces in terms of the discretized grid that is also used for the PB equation. We regard the surface in Eq. (2) as the van der Waals surface of the solute and express the surface in terms of the gradient of the volume exclusion function $H(\boldsymbol{r})$,

$$S = \int_V d^3\boldsymbol{r}\,||\nabla H||\,. \tag{21}$$

To reduce the storage requirements, the volume exclusion function in this expression can be replaced with the the associated dielectric constant defined through Eq. (5),

$$S = \left(\frac{1}{\epsilon_s - 1}\right)\int_V d^3\boldsymbol{r}\,||\nabla\epsilon||\,. \tag{22}$$

Through Eqs. (2) and (22), the nonpolar solvation force acting on atom α is

$$\mathbf{F}_\alpha^{\mathrm{NP}} = -\left(\frac{\gamma}{\epsilon_s - 1}\right)\int_V d^3\boldsymbol{r}\,\frac{\partial||\nabla\epsilon||}{\partial \boldsymbol{r}_\alpha}\,. \tag{23}$$

$\mathbf{F}_\alpha^{\mathrm{NP}}$ acts at the exposed surface of atom α to the polar solvent region to reduce the surface. Since S in Eq. (22) is a function of the shape of the solute and position of each atom of the solute, there is no analytic solution in general, except for a one atom system. However, the numerical calculation (see below) shows that the formula yields approximately the van der Waals surface of the solute, i.e., the surface formed by the overlapping atomic spheres. The current convention for calculating the nonpolar solvation free energy differs with previous treatments in which the solvent accessible surface was used [14,16,21,22]. Nevertheless, it is physically reasonable and computationally convenient because the formula for the nonpolar solvation force can easily be derived from the surface definition.

2.3. Numerical implementation

In this section, the algebraic expressions for the solvation forces are explicitly given.

Reaction field forces. In the finite-difference calculation, the atomic charge Q_α is represented by assigning fractional charges to its eight nearest grid points using a simple linear weighting function, $g(t) = (1-|t|/h)$ [2], i.e., a fractional charge of

$$q_\alpha(i,j,k) = Q_\alpha g(|x_\alpha - x_i|)g(|y_\alpha - y_j|)g(|z_\alpha - z_k|) \tag{24}$$

is assigned if (x_i, y_j, z_k) is one of the eight nearest grid points around the atomic charge Q_α. The total fractional charge at the grid point (x_i, y_j, z_k) corresponds to the superposition of the individual atomic charges of the solute,

$$q(i,j,k) = \sum_\alpha q_\alpha(i,j,k)\,. \tag{25}$$

The reaction field forces follow from the derivatives of $q(i,j,k)$ with respect to $\boldsymbol{r}_\alpha$. For example, the x-component of the reaction field force acting on atom α is given by

$$\mathbf{F}^{\mathrm{RF}}_{x\alpha} = -\sum_{\{i,j,k\}_\alpha} (\phi_\mathrm{s} - \phi_\mathrm{v})Q_\alpha \left[\frac{\partial g(|x_\alpha - x_i|)}{\partial x_\alpha}\right] g(|y_\alpha - y_j|)g(|z_\alpha - z_k|)\,, \tag{26}$$

where the derivative of the weighting function is given by

$$\frac{\partial g(|x_\alpha - x_i|)}{\partial x_\alpha} = \begin{cases} h^{-1}\,, & x_\alpha < x_i\,, \\ 0\,, & x_\alpha = x_i\,, \\ -h^{-1}\,, & x_\alpha > x_i\,. \end{cases} \tag{27}$$

The summation runs over all the nearest neighbors grid points $\{i,j,k\}_\alpha$ around the charge Q_α. Similar expressions apply for $\mathbf{F}^{\mathrm{RF}}_{y\alpha}$ and $\mathbf{F}^{\mathrm{RF}}_{z\alpha}$. It should be noted that to calculate the electrostatic solvation free energy and the reaction field forces, the PB equation must be solved twice: once for the solvent case (s) and once for the vacuum case (v). Because of the singularity in the absolute value function at $x_\alpha = x_i$, the derivative of the partial charge $q_\alpha(i,j,k)$ is always equal to zero when a particle is located at a grid point. This leads to discontinuities in the reaction field forces (see next section).

Dielectric and ionic boundary forces. According to Eqs. (5) and (7), the value of the dielectric constant and the modified Debye–Hückel screening factor is determined by the volume exclusion function, $H(\boldsymbol{r})$. In the interior of the solute, $H(\boldsymbol{r}) = 0$, whereas in the solvent region, $H(\boldsymbol{r}) = 1$. The abrupt transition of the dielectric constant function at the solute–solvent boundary gives rise to discontinuous variations of the electrostatic solvation free energies as the solute atoms are moving due to the contributions involving quantities such as $\partial\epsilon(\boldsymbol{r})/\partial\boldsymbol{r}_\alpha$. However, smooth variations of the energy are desirable in practical calculations for accurate estimates of the corresponding forces. Numerical tests indicated that a smooth boundary is necessary to make the calculated boundary forces stable. To avoid the sharp transition in the dielectric function, an intermediate dielectric region is introduced at the solute–solvent boundary. Furthermore, the extended boundary can remove small cracks and crevices in the solute that may be assigned to the high dielectric constant of the solvent and the modified Debye–Hückel screening factor at the bulk solvent [17]. The transition region is defined in terms of a simple polynomial function,

$$H_\alpha(r) = \begin{cases} 0\,, & r \le R_\alpha - w\,, \\ -\dfrac{1}{4w^3}(r - R_\alpha + w)^3 + \dfrac{3}{4w^2}(r - R_\alpha + w)^2\,, & R_\alpha - w < r < R_\alpha + w\,, \\ 1\,, & r \ge R_\alpha + w\,, \end{cases} \tag{28}$$

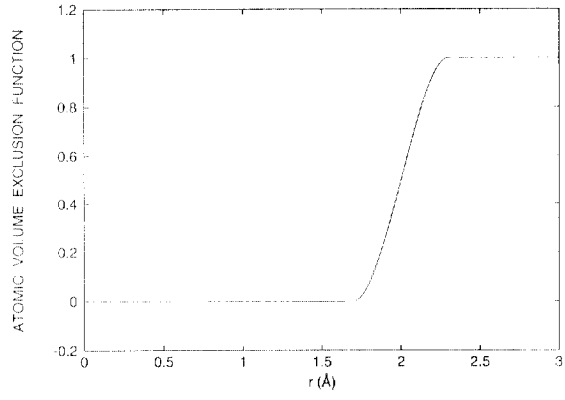

Fig. 1. Volume exclusion function of an atom having a radius of 2.0 Å for 0.3 Å smoothing window.

where r is the distance between a point on the system and atom α, R_α is the radius of atom α, and w is a smoothing window that confines the region where the smoothing function will be applied. The first derivative of the smoothing function,

$$H_\alpha'(r) = -\frac{3}{4w^3}(r - R_\alpha + w)^2 + \frac{3}{2w^2}(r - R_\alpha + w)\,, \tag{29}$$

is zero at $r = R_\alpha - w$ and $R_\alpha + w$. Fig. 1 shows a characteristic volume exclusion function of an atom having a radius of 2.0 Å for a smoothing window of 0.3 Å .

According to Eqs. (8), (15) and (18), the dielectric boundary force acting on atom α is given by

$$\begin{aligned}\mathbf{F}_\alpha^{\mathrm{DB}} = -\frac{h}{8\pi}\sum_{i,j,k}\phi_s(i,j,k)\Bigg[&\frac{\partial\epsilon_x(i,j,k)}{\partial \boldsymbol{r}_\alpha}[\phi_s(i+1,j,k)-\phi_s(i,j,k)]\\ &+\frac{\partial\epsilon_x(i-1,j,k)}{\partial \boldsymbol{r}_\alpha}[\phi_s(i-1,j,k)-\phi_s(i,j,k)]+\frac{\partial\epsilon_y(i,j,k)}{\partial \boldsymbol{r}_\alpha}[\phi_s(i,j+1,k)-\phi_s(i,j,k)]\\ &+\frac{\partial\epsilon_y(i,j-1,k)}{\partial \boldsymbol{r}_\alpha}[\phi_s(i,j-1,k)-\phi_s(i,j,k)]+\frac{\partial\epsilon_z(i,j,k)}{\partial \boldsymbol{r}_\alpha}[\phi_s(i,j,k+1)-\phi_s(i,j,k)]\\ &+\frac{\partial\epsilon_z(i,j,k-1)}{\partial \boldsymbol{r}_\alpha}[\phi_s(i,j,k-1)-\phi_s(i,j,k)]\Bigg]\,.\end{aligned} \tag{30}$$

The partial derivatives of the dielectric functions can be calculated through Eqs. (5) and (6),

$$\begin{aligned}\frac{\partial\epsilon_x(i,j,k)}{\partial \boldsymbol{r}_\alpha} &= (\epsilon_s - 1)\frac{H_x(i,j,k)}{H_{x\alpha}(i,j,k)}\frac{\partial H_{x\alpha}(i,j,k)}{\partial \boldsymbol{r}_\alpha}\\ &= (\epsilon_x(i,j,k)-1)\frac{H'_{x\alpha}(i,j,k)}{H_{x\alpha}(i,j,k)}\frac{(-\boldsymbol{r})}{r}\,,\end{aligned} \tag{31}$$

where $H_x(i,j,k)$ and $H_{x\alpha}(i,j,k)$ are the volume exclusion functions of the solute and atom α related to the x-branch of the cubic grid, i.e., at $(x_i + h/2, y_j, z_k)$. The distance r and the vector $\boldsymbol{r}$ are calculated from the center of atom α to the grid point. The expressions for the partial derivatives of ϵ_y and ϵ_z are similar.

According to Eqs. (8), (15) and (19), the ionic boundary force acting on atom α is given by

$$\mathbf{F}_\alpha^{\mathrm{IB}} = \frac{h^3}{8\pi}\sum_{i,j,k}\phi_s(i,j,k)^2\frac{\partial\bar{\kappa}^2(i,j,k)}{\partial \boldsymbol{r}_\alpha}\,, \tag{32}$$

where the derivative can be calculated through Eq. (7),

$$\frac{\partial \bar{\kappa}^2(i,j,k)}{\partial r_\alpha} = \bar{\kappa}_b^2 \frac{H(i,j,k)}{H_\alpha(i,j,k)} \frac{\partial H_\alpha(i,j,k)}{\partial r_\alpha}$$
$$= \bar{\kappa}^2(i,j,k) \frac{H'_\alpha(i,j,k)}{H_\alpha(i,j,k)} \frac{(-r)}{r}, \tag{33}$$

where $H(i,j,k)$ and $H_\alpha(i,j,k)$ are the volume exclusion functions of the solute and atom α at the grid point (x_i, y_j, z_k). The distance r and the vector r are calculated from the center of atom α to the grid point.

Nonpolar solvation forces. The van der Waals surface is defined in terms of the dielectric constants on discrete grid points,

$$S = \left(\frac{h^3}{\epsilon_s - 1}\right) \sum_{i,j,k} ||\nabla \epsilon(i,j,k)||. \tag{34}$$

The nonpolar solvation force acting on atom α, given in Eq. (23), requires the partial derivative of $||\nabla \epsilon(i,j,k)||$ with respect to the coordinate of atom α. To exploit the relationship with the grids used in the finite-difference method, this is written as

$$||\nabla \epsilon(i,j,k)|| = \sqrt{\nabla \epsilon(i,j,k) \cdot \nabla \epsilon(i,j,k)}$$
$$= h^{-1}[(\epsilon_x(i,j,k) - \epsilon_x(i-1,j,k))^2 + (\epsilon_y(i,j,k) - \epsilon_y(i,j-1,k))^2$$
$$+ (\epsilon_z(i,j,k) - \epsilon_z(i,j,k-1))^2]^{1/2}. \tag{35}$$

The nonpolar solvation force follows as

$$\mathbf{F}_\alpha^{\mathrm{NP}} = -\left(\frac{\gamma h}{\epsilon_s - 1}\right) \sum_{i,j,k} \left(\frac{1}{||\nabla \epsilon(i,j,k)||}\right) \left[[\epsilon_x(i,j,k) - \epsilon_x(i-1,j,k)] \left(\frac{\partial \epsilon_x(i,j,k)}{\partial r_\alpha} - \frac{\partial \epsilon_x(i-1,j,k)}{\partial r_\alpha}\right) \right.$$
$$+ [\epsilon_y(i,j,k) - \epsilon_y(i,j-1,k)] \left(\frac{\partial \epsilon_y(i,j,k)}{\partial r_\alpha} - \frac{\partial \epsilon_y(i,j-1,k)}{\partial r_\alpha}\right)$$
$$\left. + [\epsilon_z(i,j,k) - \epsilon_z(i,j,k-1)] \left(\frac{\partial \epsilon_z(i,j,k)}{\partial r_\alpha} - \frac{\partial \epsilon_z(i,j,k-1)}{\partial r_\alpha}\right)\right]. \tag{36}$$

The numerical calculation of $\mathbf{F}_\alpha^{\mathrm{NP}}$ is very similar to that of $\mathbf{F}_\alpha^{\mathrm{DB}}$ since the derivatives of the dielectric function in Eq. (36) are the same as in Eqs. (30) and (31). This implies that additional computing time may be saved by calculating both forces simultaneously.

3. Numerical tests and discussion

The current expressions for the calculation of the solvation forces were incorporated into the PBEQ module (Beglov and Roux, unpublished) of the biomolecular simulation program CHARMM [23]. In the following, the expression "numerically-calculated forces" refers to the results based on Eqs. (26), (30), (32), and (36). The PBEQ module of CHARMM solves the PB equation numerically using the finite-difference algorithm of Klapper et al. [2]. The calculations were performed by setting the potential at the boundary to $\psi(i,j,k) = \sum_\alpha q_\alpha/(\epsilon_s * d_\alpha(i,j,k)|) \exp[-\bar{\kappa}_b d_\alpha(i,j,k)/\sqrt{\epsilon_s}]$, where $d_\alpha(i,j,k)$ is the distance from the charge α to the (i,j,k) grid point at the boundary. Periodic boundary conditions could also be used, but the quantitative difference is

negligible for neutral solutes. Unless specified explicitly, the dielectric constant of the solvent was 80, the salt concentration 0.0 M, the smoothing window 0.3 Å, and the surface tension coefficient 0.03 kcal/(mol · Å^2).

3.1. Electrostatic solvation forces

Reaction field forces and dielectric boundary forces. The accuracy of the reaction field and dielectric boundary forces was examined in the case of a model system constituted of two particles carrying a charge of $+1.0e$. The atomic radius of both particles was 2.0 Å. One particle (A) was fixed at -3.0 Å on the x-axis and the other (B) was moved along the x-axis from 3.0 Å to -3.0 Å by small increments (δx) of 0.005 Å. The electrostatic solvation free energy and forces were calculated by solving the PB equation at every position using a $65\times65\times65$ cubic grid and a spacing of 0.21 Å. The accuracy of the solvation forces was assessed by comparing the forces calculated numerically using the expressions of Eqs. (26) and (30), with the forces calculated from a direct finite-difference of the electrostatic solvation free energies, i.e.,

$$F_x^{\text{elec-f.d.}} = -\frac{G_{\text{elec}}(x+\delta x) - G_{\text{elec}}(x-\delta x)}{2\delta x}. \tag{37}$$

Fig. 2a shows the electrostatic solvation forces of particle A (the fixed particle) and particle B (the moving particle) as a function of the coordinate of particle B. It is observed that the numerically-calculated force acting on particle B (dashed line) agrees very well with the finite-difference calculated force (dotted line). In fact, they are virtually indistinguishable. The average discrepancy is 0.05 kcal/(mol·Å) and the largest difference is 0.30 kcal/(mol·Å). The excellent agreement demonstrates the accuracy of the numerically-calculated electrostatic solvation force.

For the sake of comparison, the sign of the force acting on particle A in Fig. 2a was inverted (solid line). In a system that is perfectly invariant by translation, the forces acting on particles A and B should be the same according to Newton's third law. However, the particles experience additional forces caused by the discreteness of the grid which result in a difference between the forces acting on particles A and B. The figure also exhibits a periodic change in the force acting on particle B (the moving particle) relative to that acting on particle A (the fixed particle). The contributions of reaction field forces and dielectric boundary forces to electrostatic solvation forces are shown in Fig. 2b. As shown in the figure, the periodic variations of the electrostatic solvation force of particle B in Fig. 2a arise mainly from the dielectric boundary force and are caused by the variations in the function $\epsilon(\boldsymbol{r})$ via $H(\boldsymbol{r})$ in Eq. (5).

The reaction field forces are rigorously zero when a particle is located exactly at a lattice point (those values were omitted in both Fig. 2a and 2b for the sake of clarity). The discontinuities in the reaction field forces is due to the algorithm used to assign the partial lattice charges as can be seen from Eqs. (26) and (27). The derivative of the fractional charges distribution function g has a singularity because of the absolute value function used in the scheme. A discontinuity occurs in the corresponding force component when an atom crosses one of the face of the cubic grid (e.g., the force acting on the particle in the x direction jumps abruptly to zero when the x-coordinate of the particle is equal to the location of a grid point x_i). To avoid the discontinuous forces, it would be necessary to use a different scheme to assign the fractional charges on the grid based on the atomic position. Nevertheless, it should be stressed that the influence of the discontinuous forces is much less dramatic than could be initially assumed. First, the subspace of the configurations for which the forces are discontinuous is a set of measure zero (the discontinuities occur only when an atom is along one of the grid axis). This means that the likelihood of finding an atom at such location in the course of a simulation is negligible. Furthermore, the integral of the discontinuity is zero since the value of the force remains finite at all position. Assuming that there is a discontinuity at the point x, the work done is

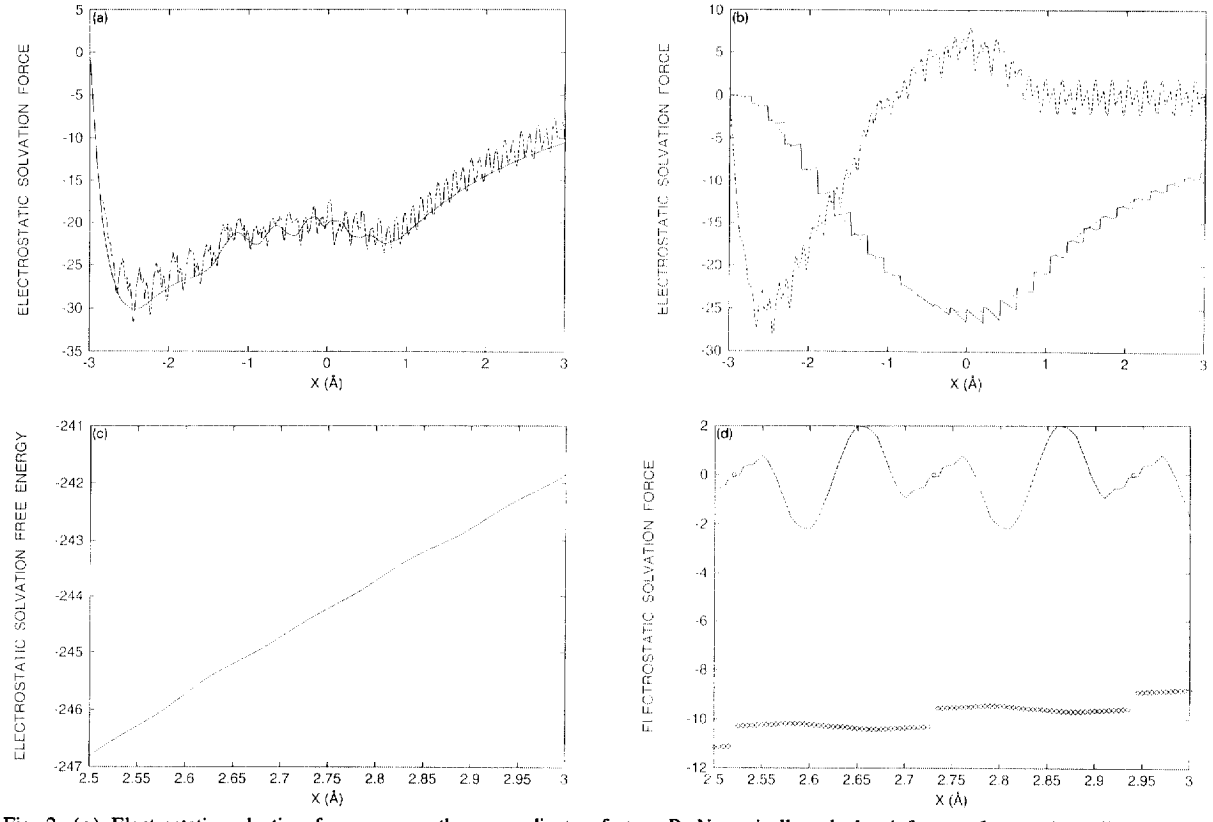

Fig. 2. (a) Electrostatic solvation forces versus the x-coordinate of atom B. Numerically calculated forces of atom A (solid line) and B (dashed line) are plotted. The finite-difference force acting on particle B (dotted line) is virtually identical to that calculated with the analytical expressions (dashed line). The sign of the forces of particle A has been inverted for the sake of comparison. All forces are expressed in kcal/(mol·Å). (b) Contributions of reaction field forces (F^{RF}) and dielectric boundary forces (F^{DB}) to electrostatic solvation forces. Reaction field forces: F_B^{RF} (solid line) and $-F_A^{\mathrm{RF}}$ (thin dashed line). Dielectric boundary forces: F_B^{DB} (heavy dashed line) and $-F_A^{\mathrm{DB}}$ (dotted line). All forces are expressed in kcal/(mol·Å). (c) Electrostatic solvation free energies (in kcal/mol) versus the x-coordinate of atom B in a subregion going from 2.5 to 3.0 Å along the x-axis. (d) Electrostatic solvation forces of atom B versus the x-coordinate of atom B in the subregion going from 2.5 to 3.0 Å along the x-axis. The dielectric boundary forces $\mathbf{F}_B^{\mathrm{DB}}$ exhibit a periodic behavior (solid line). The reaction field forces $\mathbf{F}_B^{\mathrm{RF}}$ vary discontinuously at the grid points (squares). All forces are expressed in kcal/(mol·Å).

$$\Delta G_{\mathrm{elec}} = \int_{x-0^+}^{x+0^+} F_B^{\mathrm{elec}}\, dx\,. \tag{38}$$

Therefore, the associated reversible work or free energy is continuous and the algorithm remains stable despite the spurious discontinuities in the forces. To further illustrate this point, the variations of the electrostatic solvation free energy and forces on particle B in a subregion going from 2.5 to 3.0 Å are shown in Fig. 2c and 2d. Fig. 2d shows explicitly the discontinuity of the reaction field forces (plotted as squares) which occurs at every grid point along the x-axis that results from the variations of the lattice partial charges $q(i, j, k)$. However, the electrostatic free energy shown in Fig. 2c remains very smooth despite the existence of the discontinuities.

Reaction field forces and ionic boundary forces. The accuracy of the ionic boundary forces was examined in the case of a model system constituted of one neutral particle (A) of radius of 3.0 Å and one particle (B) of

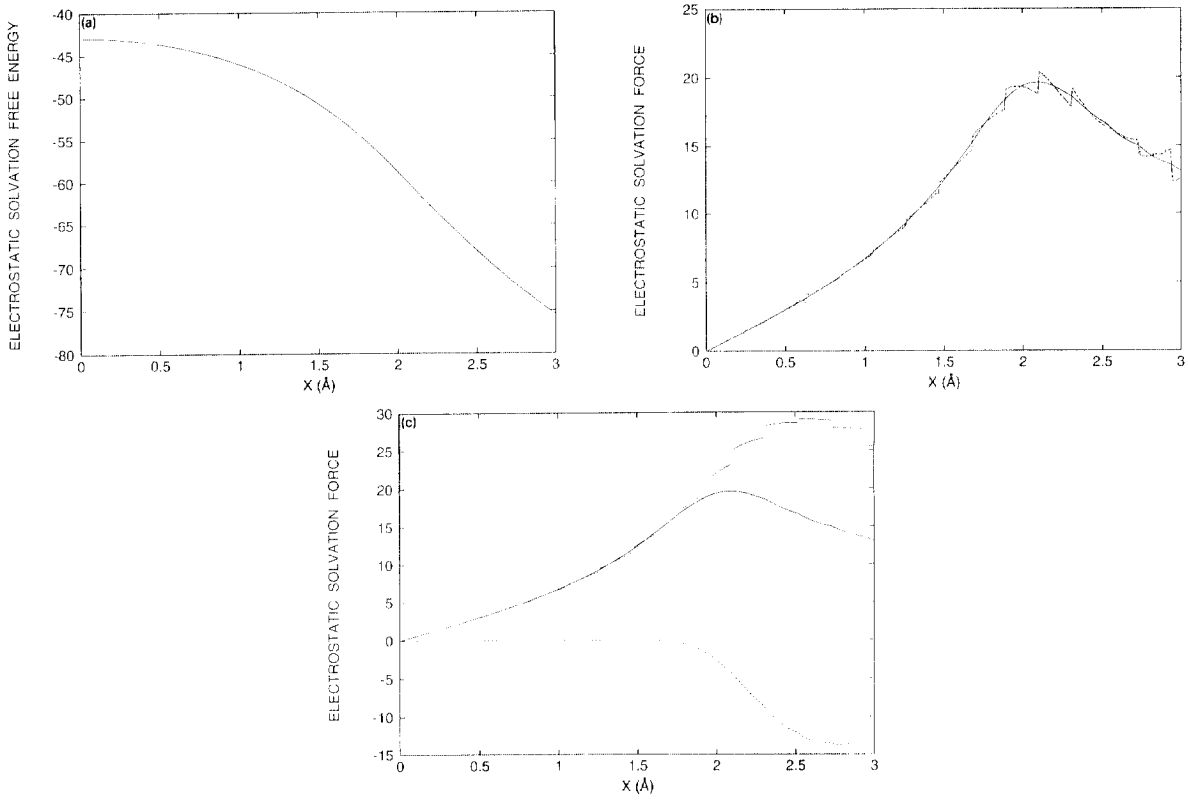

Fig. 3. (a) Electrostatic solvation free energies (in kcal/mol) versus the x-coordinate of atom B. (b) Electrostatic solvation forces versus the x-coordinate of atom B. Numerically calculated forces of atom A (solid line) and B (dashed line) are plotted. The finite-difference force acting on particle B (dotted line) is virtually identical to that calculated with the analytical expressions (dashed line). The sign of the forces of atom A has been inverted for the sake of comparison. All forces are expressed in kcal/(mol·Å) (c) Contributions of reaction field forces ($\mathbf{F}^{\mathrm{RF}}$) and ionic boundary forces ($\mathbf{F}^{\mathrm{IB}}$) to electrostatic solvation forces. Contribution of the reaction field forces acting on particle B, $\mathbf{F}_B^{\mathrm{RF}}$ (dotted line). Contribution of the ionic boundary forces acting on particle A, $\mathbf{F}_A^{\mathrm{IB}}$ (solid line) and on particle B, $\mathbf{F}_B^{\mathrm{IB}}$ (dashed line). All forces are expressed expressed in kcal/(mol·Å).

charge $+1.0e$ and radius 1.0 Å. The particle A was fixed at the origin and the particle (B) was moved along the x-axis from 0.0 Å to 3.0 Å by small increments of 0.005 Å. A salt concentration of 150 mM and a solvent dielectric constant of 1 were used. The other parameters were the same as those of the previous section. This choice of $\epsilon_s = 1$ implies that there is no dielectric boundary in the system and that all the forces are caused by the ionic boundary.

Fig. 3a shows the variations of the electrostatic solvation free energy. Fig. 3b shows the electrostatic solvation forces acting on particle A and B as a function of the position of particle B (for the sake of comparison, the sign of the force acting on particle A was inverted). It is observed that the numerically-calculated force acting on particle B (dashed line) agrees very well with the finite-difference calculated force (dotted line). The average discrepancies is 0.04 kcal/(mol·Å) and the largest difference is 0.31 kcal/(mol·Å) around $x = 0.6$ Å. The excellent agreement demonstrates the accuracy of the numerically-calculated ionic boundary forces based on Eq. (32). Fig. 3c shows the contributions of reaction field forces and ionic boundary forces to electrostatic solvation forces. All reaction field forces acting on particle B at the discontinuous points were omitted in both Fig. 3b as in Fig. 2. Periodic variations in the force acting on particle B are caused by the variations in the function $\bar{\kappa}(r)$ via $H(r)$ in Eq. (7). As in Fig. 2a, the total force acting on particle A is not exactly equal to

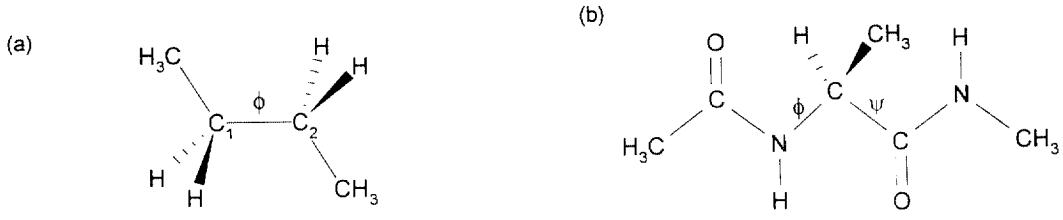

Fig. 4. The (a) *n*-butane and (b) alanine dipeptide molecules.

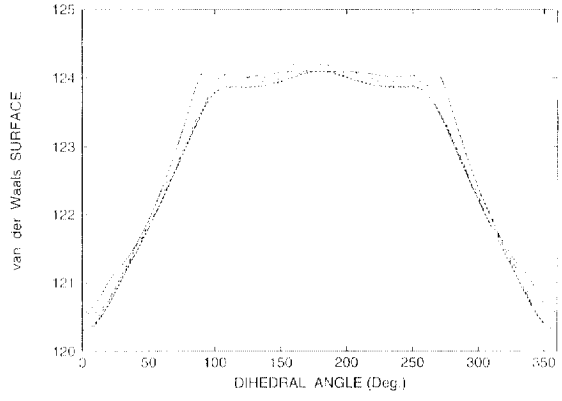

Fig. 5. The van der Waals surface (solid line) and estimated surfaces calculated with various grid spacings: 0.1 Å (heavy dashed line), 0.2 Å (thin dashed line), 0.3 Å (dotted line), 0.4 Å (heavy dot-dashed line), and 0.5 Å (thin dot-dashed line). The width of the smoothing window was 0.3 Å. All surfaces are expressed in $Å^2$.

the force acting on particle B because of the numerical grid.

It should be stressed that the large ionic boundary forces in the system result from the choice of $\epsilon_s = 1$. At a physiological salt concentration of 150 mM, the influence of the counter ions on the solvation forces is expected to be negligible relative to the dielectric boundary forces or nonpolar solvation forces [16]. For instance, if a realistic value of dielectric constant is used, the forces are reduced approximately by a factor of 80. Furthermore, except for largely charged molecules such as nucleic acid, ionic boundary forces of neutral molecules and proteins are in the range of 10^{-2} or 10^{-3} kcal/(mol·Å). This indicates that ionic boundary forces are much smaller than the dielectric boundary forces or nonpolar solvation forces in most situations.

3.2. Molecular surface and nonpolar free energy contribution

To illustrate and test the calculation of the molecular surface and the nonpolar contribution based on Eq. (22), the simple molecule *n*-butane was considered (see Fig. 4a). The numerically-calculated surface using Eq. (22) was compared with the van der Waals surface calculated by the Lee and Richards method [24] implemented in CHARMM [23]. The central dihedral angle, ϕ, was rotated from 0° to 360° by 5° with all bonds and angles fixed as their initial values and with atom C2 and C3 fixed at −0.765 Å and 0.765 Å on the *x*-axis, respectively. The molecule was modeled using the all-hydrogen PARM22 potential function [25] of CHARMM [23]. The finite-difference calculations were also carried out every step using different grid spacings (0.1, 0.2, 0.3, 0.4, and 0.5 Å). The number of grid points was chosen so that the size of the grid was about 12 Å. The width of the smoothing window was 0.3 Å.

The numerically-calculated surfaces and the van der Waals surface of *n*-butane with the central dihedral angle are shown in Fig. 5. As shown in the figure, the van der Waals surface is well-reproduced by the calculations.

As shown by the figure, the grid spacing must be smaller than the width of the smoothing window to yield an accurate estimate of the molecular surface. The dependence of the estimated surface upon the width of the smoothing window can be better understood by considering a single spherical particle of radius R_α,

$$\begin{aligned} S_\alpha &= \int_V d^3\mathbf{r}\, H'_1(|\mathbf{r}-\mathbf{r}_1|) \\ &= 4\pi \int_{R_\alpha - w}^{R_\alpha + w} H'_\alpha(r) r^2\, dr \\ &= 4\pi R_\alpha^2 \left(1 + \frac{w^2}{5R_\alpha^2}\right). \end{aligned} \tag{39}$$

The width of the smoothing region effectively increases the estimate of the molecular surface. This indicates that the nonpolar contribution to the solvation free energy must be carefully parametrized for a given value of the smoothing window. The influence of the width of the smoothing window on the calculated surface of *n*-butane was investigated. The width of the smoothing window was changed from 0.3 Å to 0.4 and 0.5 Å with a fixed grid spacing of 0.2 Å. The calculated surface are slightly shifted from 120.31 Å^2 to 121.45 and 123.03 Å^2 at $\phi = 0°$ and from 124.09, to 125.28 and 126.89 Å^2 at $\phi = 180°$. Nevertheless, the overall dependence of the energy surface as a function of the dihedral angle was almost the same as in Fig. 5 (not shown).

3.3. Dynamical simulation of alanine dipeptide

In some respect, performing a molecular dynamics simulation with the continuum solvent model constitutes the ultimate test for the current method for calculating the solvation forces. To investigate the accuracy of the solvation forces during the molecular dynamics, the alanine dipeptide molecule, shown in Fig. 4b, was considered. As a first test, we examined the accuracy of solvation forces for a set of uncorrelated configurations of alanine dipeptide. As a second test, we examined the conservation of energy during a Newtonian trajectory using the continuum solvation model.

To carry out the first test, a 100 ps trajectory of alanine dipeptide in vacuum was generated at a temperature of 1000 K. Twenty configurations of the molecule were extracted (one every 5 ps) for the force calculations. PB finite-difference calculations for solvation forces of each configuration were performed with a 75×75×75 cubic grid and a spacing of 0.20 Å. Finite-difference first derivatives were calculated with a step size of 0.001 Å. The results were compared with the results from the analytical expressions. A complete calculation for one configuration requires 264 PB calculations, i.e., the PB equation is solved for both the vacuum and solvent environments after displacing each atom by ± 0.001 Å along the three Cartesian directions from its original coordinate. The total van der Waals surface was also calculated for each configuration.

All *x*-, *y*-, and *z*-components of the calculated electrostatic and nonpolar solvation forces of each atom for 20 configurations versus the corresponding finite-difference results are shown in Figs. 6a and 6b, respectively. The line formed by each point on both figures demonstrates the excellent accuracy of the calculated solvation forces. For the electrostatic forces shown in Fig. 6a, the discrepancy is smaller than ± 0.1 kcal/(mol·Å) except for a few values. Two points are slightly off the line at about −6.0 and 4.0 kcal/(mol·Å). A closer examination of the configuration showed that the atom is very close to a grid point and that the numerical first derivatives forces were incorrectly estimated because of the rapid variation of the electrostatic solvation energy. For the nonpolar forces shown in Fig. 6b, the discrepancy between two forces ranges between $\pm 1.0 \times 10^{-5}$ kcal/(mol·Å) at all points. This negligible difference results from the fact that the calculation of nonpolar solvation forces does not depend on the convergence of electrostatic potentials. The nonpolar solvation forces are thus calculated more

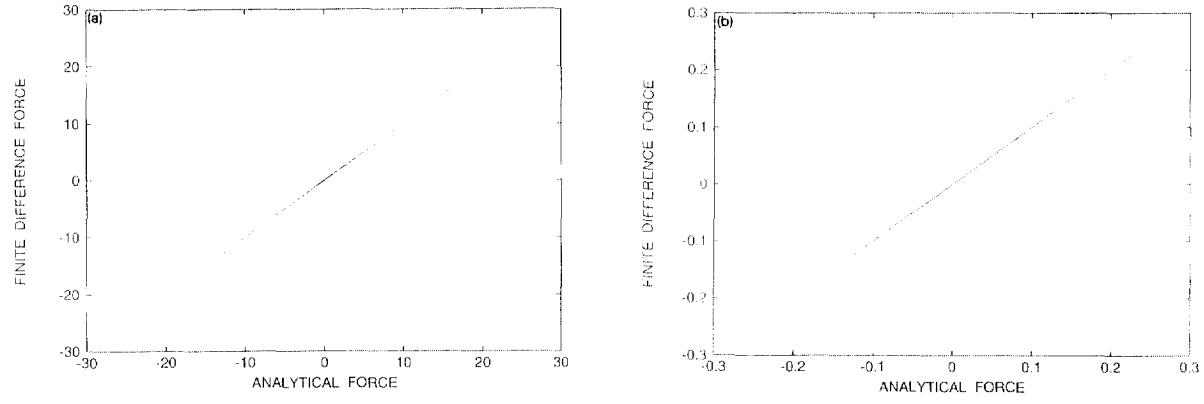

Fig. 6. Finite-difference forces compared with numerically-calculated solvation forces for 20 configurations of the alanine dipeptide molecule. The (a) electrostatic solvation forces and (b) nonpolar solvation forces are shown. The number of points on each plot is 1320 (22 × 3 × 20).

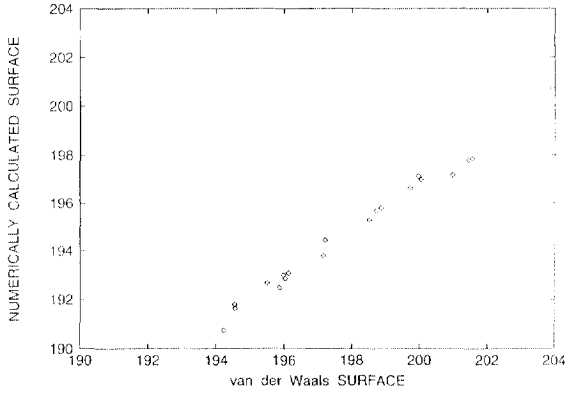

Fig. 7.

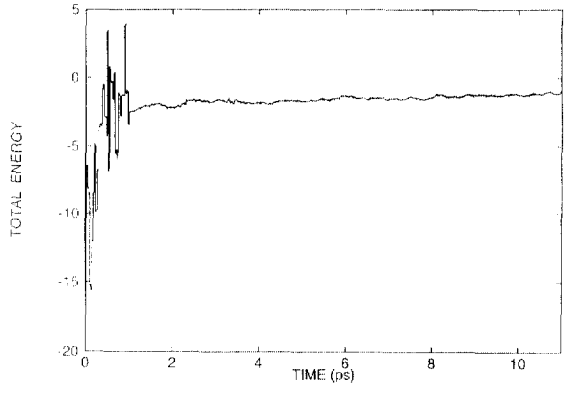

Fig. 8.

Fig. 7. Van der Waals surface versus numerically-calculated surfaces of 20 configurations of the alanine dipeptide molecule. All surfaces are expressed in $Å^2$.

Fig. 8. Total energy (in kcal/mol) during the molecular dynamics with the continuum solvation model: the equilibration run for 1 ps and the production run for 10 ps.

accurately than the electrostatic solvation forces. These results indicate that the current expressions Eqs. (26), (30), and (36), can yield very accurate solvation forces for a complex molecule.

Nonpolar solvation forces and dielectric boundary forces are much smaller than reaction field forces. All of investigated nonpolar solvation forces ranged between ± 0.3 kcal/(mol·Å) and dielectric boundary forces almost lay between ± 0.5 kcal/(mol·Å), whereas reaction field forces followed a Gaussian-like distribution (not shown) with a standard deviation of ± 18.0 kcal/(mol·Å). The calculated surfaces and van der Waals surfaces are shown in Fig. 7 for 20 configurations. Although the figure indicates that there can be small deviations, the standard van der Waals surfaces are generally well reproduced by Eq. (22).

As a final test, the total energy was monitored during a molecular dynamics trajectory with continuum solvation free energy. The initial coordinates of alanine dipeptide obtained from its standard parameters were first optimized with energy minimization. The molecule was modeled using the all-hydrogen PARM22 potential function [25] of CHARMM [23]. An equilibration run was then carried out for 1 ps followed by a production

run for 10 ps using the Verlet algorithm with a time step of 0.001 ps. The PB equation was solved every dynamical step along the trajectory using a $65\times65\times65$ grid with a spacing of 0.25 Å. The solvation forces were recalculated at every dynamical step. A harmonic potential was applied to the center of mass of the molecule to prevent any global translation during the trajectory. Fig. 8 shows the total energy during the molecular dynamics with the continuum solvation model. During the equilibration run, total energy changes rapidly because of the reassignment of the velocities of each atom every 25 step. After 2.5 ps, the total energy is well conserved, even though a slight increase of the total energy is observed. This indicates that the solvation forces are calculated accurately during the trajectory based on the continuum solvation model.

4. Summary

A rigorous formulation for the calculation of electrostatic solvation forces was developed from the linearized Poisson–Boltzmann (PB) equation. Although the expressions for the solvation forces were developed in the case of the finite-difference algorithm described by Eq. (8), it should be stressed that the present approach based on the formal solution of Eq. (9) is general and could be used in the case of other numerical algorithm for solving the PB equation (4). The solute–solvent boundary was constructed on the basis of a volume exclusion function defined in terms of overlapping radial atom-centered smooth functions. The introduction of a smooth solute–solvent boundary was required to improve the stability and the accuracy of the force calculations during molecular mechanics trajectories. The nonpolar contribution to the solvation free energy was expressed in terms of a volume integral of the modulus of the gradient of the dielectric function. The calculation of the nonpolar contribution to the solvation free energy, done on the basis of the existing grid mapping of the dielectric function, decreases the storage requirements and saves additional computing time by avoiding an external calculations of the molecular surface. A series of accuracy tests showed that the numerically-calculated solvation forces were consistent with the first derivative of the solvation free energy obtained from finite difference. As a final test of the method, a molecular dynamics simulation of the alanine dipeptide was performed. It was observed that energy was well-conserved during the trajectory.

Significant difficulties still restrict the application of continuum electrostatics in molecular dynamics simulations of proteins and biomolecules. Firstly, it is essential to obtain free energies of solvation that are in quantitative agreement with experimental values for meaningful calculations. Since no systematic efforts were made to optimize the atomic radii, the surface tension coefficient and the width of the smoothing window used in this paper, the calculations described above have only an illustrative purpose. Preliminary tests indicate that the value of the solvation free energy depends both on the atomic radii and on the width of the smoothing window. Extended atomic radii for PB calculations taking into account the width of the smoothing window are currently being developed on the basis of the electrostatic solvation free energy of the 20 standard amino acids calculated by free energy simulation techniques with explicit water molecules [9]. Subsequently, the combined influence of the grid spacing and the width of the smoothing window on the solvation free energy and accuracy of the forces will be assessed. Secondly, the computational effort required for the solution of the PB equation still restricts its application to generate trajectories. Our current finite-difference algorithm requires about 55 s (CPU time) on a SGI R10000 for a $65 \times 65 \times 65$ grid for one calculation cycle of the free energy and forces; the simulation of the alanine dipeptide takes about 15.5 CPU hours for 1 ps. Even though additional computer time can be saved by performing the calculations of the forces every 5 or 10 steps, the approach remains prohibitively slow. Further work will be devoted to improvements of the numerical algorithms for solving the PB equation numerically.

Acknowledgements

This work was supported by NSERC. B.R. is a MRC research fellow. W.I. has a studentship from the University of Montreal.

References

[1] J. Warwicker, H.C. Watson, J. Mol. Biol. 157 (1982) 671.
[2] I. Klapper, R. Hagstrom, R. Fine, K. Sharp, B. Honig, Proteins 1 (1986) 47.
[3] K.A. Sharp, B. Honig, Ann. Rev. Biophys. Chem. 19 (1990) 301.
[4] D. Bashford, M. Karplus, Biochemistry 29 (1990) 10219.
[5] A. Jean-Charles, A. Nicholls, K. Sharp, B. Honig, A. Tempczyk, T. Hendrickson, W.C. Still, J. Am. Chem. Soc. 113 (1991) 1454.
[6] B. Honig, A. Nicholls, Science 268 (1995) 1144.
[7] M.K. Gilson, Curr. Opin. Struct. Biol. 5 (1995) 216.
[8] S.R. Edinger, C, Cortis, P.S. Shenkin, R.A. Friesner, J. Phys. Chem. B 101 (1997) 1190.
[9] M. Nina, D. Beglov, B. Roux, Atomic radii for continuum electrostatics calculations based on molecular dynamics free energy simulations, J. Phys. Chem. B 101 (1997) 5239.
[10] D. Beglov, B. Roux, J. Chem. Phys. 104 (1996) 8678.
[11] M.P. Allen, D.J. Tildesley, Computer Simulation of Liquids (Oxford Science Publications, Clarendon Press, Oxford, 1989).
[12] J.L. Smart, T.J. Marrone, J.A. McCammon, J. Comput. Chem. 18 (1997) 1750.
[13] M.E. Davis, J.A. McCammon, J. Comput. Chem. 11 (1990) 401.
[14] K. Sharp, J. Comput. Chem. 12 (1991) 454.
[15] C. Niedermeier, K. Schulten, Mol. Simul. 8 (1992) 361.
[16] M.K. Gilson, M.E. Davis, B.A. Luty, J.A. McCammon, J. Phys. Chem. 97 (1993) 3591.
[17] M.K. Gilson, J.A. McCammon, J.D. Madura, J. Comput. Chem. 16 (1995) 1081.
[18] R.J. Zauhar, R.S. Morgan, J. Mol. Biol. 186 (1985) 815.
[19] B.J. Yoon, A.M. Lenhoff, J. Phys. Chem. 12 (1992) 575.
[20] B. Roux, Biophys. J. (1997).
[21] R.B. Hermann, J. Phys. Chem. 76 (1972) 2754.
[22] T. Simonson, A. Brunger, J. Phys. Chem. 98 (1994) 4683.
[23] B.R. Brooks, R.E. Bruccoleri, B.D. Olafson, D.J. States, S. Swaminathan, M. Karplus, CHARMM: A program for macromolecular energy minimization and dynamics calculations, J. Comput. Chem. 4 (1983) 187.
[24] B. Lee, F.M. Richards, J. Mol. Biol. 55 (1971) 379.
[25] A.D. Mackerell Jr., D. Bashford, M. Bellot, R.L. Dunbrack, M.J. Field, S. Fischer, J. Gao, H. Guo, D. Joseph, S. Ha, L. Kuchnir, K. Kuczera, F.T.K. Lau, C. Mattos, S. Michnick, D.T. Nguyen, T. Ngo, B. Prodhom, B. Roux, B. Schlenkrich, J. Smith, R. Stote, J. Straub, J. Wiorkiewicz-Kuczera, M. Karplus, Biophys. J. 61 (1992) A143.